A. Carpio* and E. Cebrian

# Positivity preserving high order schemes for angiogenesis models

https://doi.org/10.1515/ijnsns-2021-0112
Received March 17, 2021; accepted March 17, 2021; published online April 9, 2021

**Abstract:** Hypoxy induced angiogenesis processes can be described by coupling an integrodifferential kinetic equation of Fokker–Planck type with a diffusion equation for the angiogenic factor. We propose high order positivity preserving schemes to approximate the marginal tip density by combining an asymptotic reduction with weighted essentially non oscillatory and strong stability preserving time discretization. We capture soliton-like solutions representing blood vessel formation and spread towards hypoxic regions.

**Keywords:** angiogenesis; asymptotic reduction; Fokker–Planck; high order schemes; kinetic models; positivity preserving.

## 1 Introduction

Angiogenesis is a physiological process through which new blood vessels originate from pre-existing ones [1, 2], by sprouting and splitting. Blood vessel development is a normal and vital process in tissue growth, development and repair. However, it is also essential in the transition of tumors, from a benign to a malignant state [3], and in many inflammatory and immune diseases. Some treatments rely on the use of angiogenesis inhibitors [2, 4–6]. Angiogenesis is related to hypoxia, that is, low levels of oxygen. Cells in hypoxic regions release substances, such as VEGF (vascular endothelial growth factor), which diffuse reaching adjacent blood vessels. VEGF has been shown to increase the number of capillaries in a given network. In its presence, endothelial cells proliferate and migrate, eventually creating tubular structures resembling capillaries [7]. Figure 1 illustrates the process.

Many models dealing with different features of angiogenesis processes have been proposed, see [8–12] for instance. Nevertheless, new experimental observations inspire novel mathematical models focusing on new features. The ultimate goal is to control the angiogenesis process to help healing as well as healthy tissue development. Kinetic models allow us to gain insight on the dynamics of blood vessel networks by means of asymptotic and numerical tools. We consider a kinetic model, which describes the stochastic nature of blood vessel branching, derived from stochastic representations of the formation of blood vessel networks by means of ensemble averages [13]. Let us denote by $p$ and $C$, the density of actively moving blood vessel tips and the concentration of angiogenic factor released by hypoxic cells, respectively. Their time evolution is governed by the following system of nondimensional equations:

$$\begin{aligned}\frac{\partial}{\partial t}p\left(\mathbf{x},\mathbf{v},t\right)=\alpha\left(C\left(\mathbf{x},t\right)\right)\delta_{\sigma_v}\left(\mathbf{v}-\mathbf{v}^0\right)p\left(\mathbf{x},\mathbf{v},t\right)-\Gamma p\left(\mathbf{x},\mathbf{v},t\right)\int_0^t \mathrm{d}s\int \mathrm{d}\mathbf{v}' p(\mathbf{x},\mathbf{v}',s)\\ -\mathbf{v}\cdot\nabla_{\mathbf{x}}p(\mathbf{x},\mathbf{v},t)+\beta\mathrm{div}_{\mathbf{v}}(\mathbf{v}p(\mathbf{x},\mathbf{v},t))\\ -\mathrm{div}_{\mathbf{v}}\left[\beta\mathbf{F}\left(C(\mathbf{x},t)\right)p(\mathbf{x},\mathbf{v},t)\right]+\frac{\beta}{2}\Delta_{\mathbf{v}}p(\mathbf{x},\mathbf{v},t),\end{aligned}\tag{1}$$

***Corresponding author**: **A. Carpio**, Departamento de Matematica Aplicada, Universidad Complutense, 28040 Madrid, Spain, E-mail: carpio@mat.ucm.es
**E. Cebrian**, Departamento de Matematicas y Computación, Universidad de Burgos, 09001 Burgos, Spain

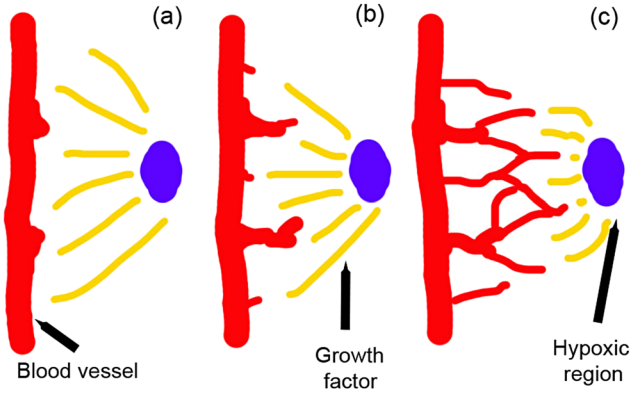


**Figure 1:** Schematic illustration of the angiogenesis process: (a) the growth factor released by the hypoxic region reaches an existing blood vessel. (b) Tip cells lead the formation of new vessels. (c) The new vessels branch and spread towards the hypoxic region.

$$\frac{\partial}{\partial t}C(\mathbf{x},t) = \kappa\Delta_{\mathbf{x}}C(\mathbf{x},t) - \chi C(\mathbf{x},t)j(\mathbf{x},t), \tag{2}$$

$$p(\mathbf{x},\mathbf{v},0) = p_0(\mathbf{x},\mathbf{v}), \quad C(\mathbf{x},0) = C_0(\mathbf{x}), \tag{3}$$

where

$$\alpha(C(\mathbf{x},t)) = A\frac{C(\mathbf{x},t)}{1+C(\mathbf{x},t)}, \quad \mathbf{F}(C(\mathbf{x},t)) = \frac{\delta_1}{(1+\Gamma_1 C(\mathbf{x},t))^{q_1}}\nabla_{\mathbf{x}}C(\mathbf{x},t), \tag{4}$$

$$j(\mathbf{x},t) = \int_{\mathbb{R}^N}\frac{|\mathbf{v}|}{1+\mathrm{e}^{(|\mathbf{v}-\mathbf{v}^0|^2-\eta)/\epsilon}}p(\mathbf{x},\mathbf{v},t)\mathrm{d}\mathbf{v}, \rho(\mathbf{x},t) = \int_{\mathbb{R}^N}p(\mathbf{x},\mathbf{v},t)\mathrm{d}\mathbf{v}, \tag{5}$$

for $\mathbf{x}\in\Omega\subset\mathbb{R}^N$, $\mathbf{v}\in\mathbb{R}^N$, $N=2$, $t\in[0,\infty)$. The term $\alpha(C)\delta_{\sigma_v}p$ represents the creation of new tips, while $-\Gamma p\int_0^t\rho\,\mathrm{d}s$ quantifies tip destruction when existing vessels merge. The Fokker–Planck operator represents vessel branching and spreading. The presence of the force term $\mathbf{F}(C)$ in Eq. (1) for the tip density $p$ forces spreading towards the region where the source of growth factor is located. Similarly, the nonlocal sink $-Cj$ in (2) represents consumption of growth factor by the created vessel tips. The dimensionless parameters $\beta$, $\Gamma$, $\kappa$, $\chi$, $A$, $\Gamma_1$, $\delta_1$, $\eta$, $\epsilon$ and $q_1$ are positive. $\delta_{\sigma_v}$ is a regularization of a delta function, a Gaussian centered about a reference velocity $\mathbf{v}_0$:

$$\delta_{\sigma_v}(\mathbf{v}-\mathbf{v}_0) = \frac{1}{\pi\sigma_v^2}\mathrm{e}^{-|\mathbf{v}-\mathbf{v}_0|^2/\sigma_v^2}. \tag{6}$$

An existence, stability and regularity theory in bounded and unbounded domains is developed in [14, 15]. Approximate soliton-like wave solutions have been found for the density of tips, which emerge at a pre-existing blood vessel and advance until the hypoxic region is reached [16, 17]:

$$\begin{aligned}\rho_s(x_1;K,c,X) &= \frac{(2K\Gamma+\mu^2)c}{2\Gamma(c-F_1)}\mathrm{sech}^2\left[\frac{\sqrt{2K\Gamma+\mu^2}}{2(c-F_1)}(x_1-X)\right],\\ \dot{X} &= \frac{\mathrm{d}X}{\mathrm{d}t} = c,\end{aligned} \tag{7}$$

where $c$ denotes the propagation speed and $X(t)$, the position of the maximum. Under some hypotheses, the parameters $K$ and $c$ satisfy a complementary set of equations.

We focus here in two-dimensional settings, where these models may be adapted to describe angiogenesis disorders causing retinopathies [18], for instance. In three dimensions, the nonlocal terms must be modified to account for the three dimensional peculiarities of blood vessel interaction and high order schemes would be necessary to reproduce such complex interactions. This task may involve a large computational cost due to the presence of both space and velocity variables. Since the solutions of the model represent densities

and concentrations, it is essential to use numerical discretizations ensuring positivity, a general issue with kinetic descriptions, which is challenging due to the presence of nonlocal terms and sources whose sign may change [17].

Finite difference and finite element schemes for Vlasov–Fokker–Planck models are considered in [19–21]. Note that system (1)–(5) resembles Vlasov–Poisson–Fokker–Planck (VPFP) equations except for the coupling with a diffusion problem and the presence of a nonlocal in time sink. In higher dimensions, random particle methods [22] and deterministic particle methods combined with splitting of diffusion and convection operators [23], have been proposed, as well as finite difference schemes combined with a change of variables [24]. These schemes are usually tested tracking convergence to a stationary solution, under periodic boundary conditions to simplify.

Schemes for other kinetic problems exploit their specific features [25]. For Vlasov–Poisson (VP) and Vlasov–Maxwell (VM) systems, [26] gives an overview of possible approaches: WENO interpolation [27], discontinuous Galerkin techniques [28], conservative flux based methods [29], energy conserving finite differences [30], particle in cell techniques [31, 32] and semi-Lagrangian approaches [33] generalizing splitting methods [34] are the typical options. VM and VP models involve transport operators coupled to either Maxwell or Poisson problems. They lack the degenerate diffusion term part of Fokker–Planck (FP) operators. In several dimensions, numerical schemes for Fokker–Planck equations are proposed in [35, 36], for instance; they often use finite differences [37]. Variants of the Fokker–Planck operators are studied in [38, 39].

High order schemes for multidimensional VP and VPFP problems include approaches based on finite volume methods [40], semi-Lagrangian discretization [41] or mesh free techniques [42]. In the slab geometry, for (1)–(5), we consider that finite differences constitute a robust choice to preserve positivity and tackle the nonlocal in time coefficients, as well as the coupling with the diffusion equation. Our goal here is to devise high order schemes. To lower the computational cost, we consider the limit of large $\beta$ and work with an asymptotic approximation of the full model which provides reduced equations for key magnitudes: the marginal tip density and the angiogenic factor concentration. We will focus on the final system, which does not depend on the velocity, combining positivity preserving weighted essentially nonoscillatory (WENO) discretizations of the differential operators in space and adequate strong stability preserving (SSP) discretizations in time [43–46].

The paper is organized as follows. Section 2 presents the two dimensional reduction of the full model. Sections 3 and 4 provide details on the spatial discretization by means of WENO and SSP schemes. Section 5 displays numerical solutions representing the blood vessel tips migrating towards a hypoxic region. Finally, Section 6 contains our conclusions.

## 2 Asymptotic reduction

In the limit of large friction, $\beta \to \infty$, the kinetic equation can be approximated by a reduced equation for the marginal density (5). The source terms in Eq. (1) (two first terms on its right-hand side) favor velocities in a small neighborhood of $\mathbf{v}^0$. Such velocities are those for which the tip creation term proportional to $\alpha(C)\delta_{\sigma_v}(\mathbf{v}-\mathbf{v}^0)$ may balance the nonlocal tip destruction sink term $-\Gamma p \int_0^t \rho\, \mathrm{d}s$. A reduced equation for $\rho$ is obtained by the Chapman–Enskog method [16].

In the limit as $\beta \to \infty$, the marginal density $\rho(\mathbf{x}, t)$ and the concentration $C(\mathbf{x}, t)$ obey the equations [17]:

$$\frac{\partial \rho}{\partial t} + \mathrm{div}_{\mathbf{x}}(\mathbf{F}\rho) - \frac{1}{2\beta}\Delta_{\mathbf{x}}\rho = \mu\,\rho - \Gamma\rho \int_0^t \rho(\mathbf{x}, s)\mathrm{d}s, \tag{8}$$

$$\mu = \frac{\alpha}{\pi}\left[1 + \frac{\alpha}{2\pi\beta(1+\sigma_v^2)}\ln\left(1+\frac{1}{\sigma_v^2}\right)\right], \tag{9}$$

$$\frac{\partial}{\partial t}C(\mathbf{x}, t) = \kappa\Delta_{\mathbf{x}}C(\mathbf{x}, t) - \chi_1\, C(\mathbf{x}, t)\rho(\mathbf{x}, t), \tag{10}$$

$$\chi_1 = \frac{\chi}{\pi}\int_0^{\infty}\int_{-\pi}^{\pi}\frac{\sqrt{1+V^2+2V\cos\varphi}}{1+\mathrm{e}^{(V^2-\eta)/\epsilon}}\mathrm{e}^{-V^2}V\,\mathrm{d}V\,\mathrm{d}\varphi. \tag{11}$$

To leading order, the marginal density and the density are related by

$$p(\mathbf{x},\mathbf{v},t) \sim \frac{1}{\pi}\mathrm{e}^{-|\mathbf{v}-\mathbf{v}_0|^2}\rho(\mathbf{x},t). \tag{12}$$

A positivity preserving order one scheme would follow by explicit forward time discretization, upwind treatment of transport terms and centered schemes for Laplacians. Integral terms can be discretized using composite Simpson rules.

To obtain a higher order scheme, we resort to positivity preserving WENO5 schemes for spatial operators, introduced in [43] for conservation laws with nonlinear fluxes and divergence free advection. Reference [43] starts from Lax–Friedrichs fluxes, we will use upwind fluxes here instead, and adapt the schemes to advection terms not necessarily divergence free. Also, the integral $I(\mathbf{x},t)=\int_0^t\rho(\mathbf{x},s)\mathrm{d}s$ becomes an additional equation

$$I'(\mathbf{x},t)=\rho(\mathbf{x},t),\quad I(\mathbf{x},0)=0. \tag{13}$$

The final system is composed of two equations involving diffusion, reaction and convection terms, coupled to this additional ordinary differential equation. In the next section, we detail the spatial discretization procedure.

# 3 Weighted essentially non oscillatory space discretization

Let us consider a two dimensional convection–diffusion problem of the form

$$u_t+(au)_x+(bu)_y-d(u_{xx}+u_{yy})=h(u), \tag{14}$$

where $d$ is a constant, either $d>0$ or $d=0$, and $\mathbf{c}=(a,b)$. In our case, $\mathbf{c}=\mathbf{F}=(F_1,F_2)$ depends on $\mathbf{x}=(x,y)$, and it is not necessarily divergence free.

Let us introduce a uniform rectangular mesh $(x_i,y_j)$, with $x_{i+\frac{1}{2}}=x_{\frac{1}{2}}+i\delta x$, $i=0,\dots,N_x$ and $y_{j+\frac{1}{2}}=y_{\frac{1}{2}}+j\delta y$, $j=0,\dots,N_y$. Let us denote the midpoints by $x_i=\frac{x_{i-\frac{1}{2}}+x_{i+\frac{1}{2}}}{2}$ and $y_j=\frac{y_{j-\frac{1}{2}}+y_{j+\frac{1}{2}}}{2}$. The spatial steps are given by $\delta x=X/N_x$ and $\delta y=Y/N_y$ for intervals $[0,X]$, $[0,Y]$. Several schemes for one dimensional conservations laws and for two-dimensional nonlinear laws as well as advection equations with divergence free non smooth velocities are described in [43]. We specify here the procedure we use for our two-dimensional operators with not necessarily divergence free advection coefficients, adapted from [43] with upwind fluxes, instead of Lax–Friedrichs.

**Step 1. Integrate (14) in the cell $C_{ij}=[x_{j-\frac{1}{2}}x_{j+\frac{1}{2}}]\times[y_{j-\frac{1}{2}}y_{j+\frac{1}{2}}]$.** To handle the possible presence of a diffusive term, double cell averages are used:

$$\overline{\overline{u}}_{ij}=\frac{1}{\delta x^2\delta y^2}\int_{y_{j-\frac{1}{2}}}^{y_{j+\frac{1}{2}}}\int_{y-\frac{\delta y}{2}}^{y+\frac{\delta y}{2}}\int_{x_{i-\frac{1}{2}}}^{x_{i+\frac{1}{2}}}\int_{x-\frac{\delta x}{2}}^{x+\frac{\delta x}{2}}u(\xi,\eta)\mathrm{d}\xi\,\mathrm{d}x\,\mathrm{d}\eta\,\mathrm{d}y. \tag{15}$$

Integrating we find:

$$\begin{aligned}\frac{\mathrm{d}\,\overline{\overline{u}}_{ij}}{\mathrm{d}t} &= -\frac{1}{\delta x^2\delta y^2}\int_{y_{j-\frac{1}{2}}}^{y_{j+\frac{1}{2}}}\int_{y-\frac{\delta y}{2}}^{y+\frac{\delta y}{2}}\left[\int_{x_i}^{x_{i+1}} au\,\mathrm{d}x - \int_{x_{i-1}}^{x_i} au\,\mathrm{d}x\right]\mathrm{d}\eta\,\mathrm{d}y\\ &\quad - \frac{1}{\delta x^2\delta y^2}\int_{x_{i-\frac{1}{2}}}^{x_{i+\frac{1}{2}}}\int_{x-\frac{\delta x}{2}}^{x+\frac{\delta x}{2}}\left[\int_{y_j}^{y_{j+1}} bu\,\mathrm{d}y - \int_{y_{j-1}}^{y_j} bu\,\mathrm{d}y\right]\mathrm{d}\xi\,\mathrm{d}x\\ &\quad + \frac{d}{\delta x^2\delta y^2}\int_{y_{j-\frac{1}{2}}}^{y_{j+\frac{1}{2}}}\int_{y-\frac{\delta y}{2}}^{y+\frac{\delta y}{2}}[u(x_{i+1},\eta) - 2u(x_i,\eta) + u(x_{i-1},\eta)]\,\mathrm{d}\eta\,\mathrm{d}y\\ &\quad + \frac{d}{\delta x^2\delta y^2}\int_{x_{i-\frac{1}{2}}}^{x_{i+\frac{1}{2}}}\int_{x-\frac{\delta x}{2}}^{x+\frac{\delta x}{2}}[u(\xi,y_{j+1}) - 2u(\xi,y_j) + u(\xi,y_{j-1})]\,\mathrm{d}\xi\,\mathrm{d}x\\ &\quad + \frac{1}{\delta x^2\delta y^2}\overline{\overline{h(u)}}_{ij}.\end{aligned} \tag{16}$$

**Step 2: Replace the integrals by quadrature rules of 5-th order**. Three-point Legendre–Gauss quadrature rules are the standard choice. The weights and nodes are:

$$\begin{aligned} x_\gamma &= \left\{-\frac{\sqrt{15}}{10}, 0, \frac{\sqrt{15}}{10}\right\}, \quad w_\gamma = \left\{\frac{5}{18}, \frac{4}{9}, \frac{5}{18}\right\}, \quad \text{in}[-1/2, 1/2],\\ x_{i+1}^\gamma &= x_{i+1} + x_\gamma\delta x, \qquad\qquad w_\gamma, \qquad\qquad \text{in}[x_i, x_{i+1}],\end{aligned} \tag{17}$$

with $\gamma = 1, 2, 3$. For these double integrals

$$\begin{aligned}\frac{1}{\delta x^2}\int_{x_{i-\frac{1}{2}}}^{x_{i+\frac{1}{2}}}\int_{x-\frac{\delta x}{2}}^{x+\frac{\delta x}{2}} v(\xi)\mathrm{d}\xi\,\mathrm{d}x &= \frac{1}{\delta x}\sum_{\gamma=1}^{3}\omega_\gamma\int_{x_i+x_\gamma\delta x-\frac{\delta x}{2}}^{x_i+x_\gamma\delta x+\frac{\delta x}{2}} u(\xi)\mathrm{d}\xi\\ &= \sum_{\gamma=1}^{3}\sum_{\gamma'=1}^{3}\omega_\gamma\omega_{\gamma'}v(x_i + x_\gamma\delta x + x_{\gamma'}\delta x) = \sum_{\gamma=1}^{5}\tilde{w}_\gamma v(\tilde{x}_i^\gamma),\end{aligned} \tag{18}$$

where the final nodes $\tilde{x}_i^\gamma$ and weights $\tilde{w}_\gamma$ are

$$\begin{aligned}&\left\{x_i - \frac{\sqrt{15}}{5}\delta x,\ x_i - \frac{\sqrt{15}}{10}\delta x,\ x_i,\ x_i + \frac{\sqrt{15}}{10}\delta x,\ x_i + \frac{\sqrt{15}}{5}\delta x\right\},\\ &\left\{w_1^2,\ 2w_1w_2,\ 2w_1w_3 + w_2^2,\ 2w_3w_2,\ w_3^2\right\},\end{aligned} \tag{19}$$

with $\gamma = 1, \ldots, 5$. Using these quadrature rules, (16) becomes

$$\begin{aligned}\frac{\mathrm{d}\,\overline{\overline{u}}_{ij}}{\mathrm{d}t} &= -\frac{1}{\delta x}\sum_{\alpha=1}^{5}\sum_{\beta=1}^{3}\tilde{w}_\alpha w_\beta\left[au\left(x_{i+\frac{1}{2}}^\beta, \tilde{y}_j^\alpha\right) - au\left(x_{i-\frac{1}{2}}^\beta, \tilde{y}_j^\alpha\right)\right]\\ &\quad - \frac{1}{\delta y}\sum_{\alpha=1}^{5}\sum_{\beta=1}^{3}\tilde{w}_\alpha w_\beta\left[bu\left(\tilde{x}_i^\alpha, y_{j+\frac{1}{2}}^\beta\right) - bu\left(\tilde{x}_i^\alpha, y_{j-\frac{1}{2}}^\beta\right)\right]\\ &\quad + \frac{d}{\delta x^2}\sum_{\alpha=1}^{5}\tilde{w}_\alpha\left[u(x_{i+1}, \tilde{y}_j^\alpha) - 2u(x_i, \tilde{y}_j^\alpha) + u(x_{i-1}, \tilde{y}_j^\alpha)\right]\\ &\quad + \frac{d}{\delta y^2}\sum_{\alpha=1}^{5}\tilde{w}_\alpha\left[u(\tilde{x}_i^\alpha, y_{j+1}) - 2u(\tilde{x}_i^\alpha, y_j) + u(\tilde{x}_i^\alpha, y_{j-1})\right]\\ &\quad + \sum_{\alpha=1}^{5}\sum_{\beta=1}^{5}\tilde{w}_\alpha\tilde{w}_\beta h(\tilde{x}_i^\alpha, \tilde{y}_j^\beta).\end{aligned} \tag{20}$$

**Step 3. Upwinding in the advection terms**. To ensure stability and preserve positivity, it is convenient to discretize the advection terms in such a way that information follows the characteristics [17, 43], that is achieved by rewriting the terms $au(x^\beta_{i+\frac{1}{2}}, \tilde{y}^\alpha_j)$, $bu(\tilde{x}^\alpha_j, y^\beta_{i+\frac{1}{2}})$ in terms of numerical fluxes that are consistent with the physical flux. In the absence of diffusion and sources, this choice would also ensure that the scheme is conservative: speeds and possible shocks would be correctly captured. In this paper we use generalize upwind fluxes. Setting $f(u) = au$, we replace $au(x^\beta_{i+\frac{1}{2}}, \tilde{y}^\alpha_j)$ by

$$\hat{f}\left(u\left(x^\beta_{i+\frac{1}{2}}, \tilde{y}^\alpha_j\right)^-, u\left(x^\beta_{i+\frac{1}{2}}, \tilde{y}^\alpha_j\right)^+\right) = \begin{cases} a\left(x^\beta_{i+\frac{1}{2}}, \tilde{y}^\alpha_j\right) u\left(x^\beta_{i+\frac{1}{2}}, \tilde{y}^\alpha_j\right)^-, a\left(x^\beta_{i+\frac{1}{2}}, \tilde{y}^\alpha_j\right) \geq 0, \\ a\left(x^\beta_{i+\frac{1}{2}}, \tilde{y}^\alpha_j\right) u\left(x^\beta_{i+\frac{1}{2}}, \tilde{y}^\alpha_j\right)^+, a\left(x^\beta_{i+\frac{1}{2}}, \tilde{y}^\alpha_j\right) < 0, \end{cases} \tag{21}$$

where $u(x^\beta_{i-\frac{1}{2}}, \cdot)^+$ and $u(x^\beta_{i+\frac{1}{2}}, \cdot)^-$ are the approximations of $u(x^\beta_{i-\frac{1}{2}}, \cdot)$ and $u(x^\beta_{i+\frac{1}{2}}, \cdot)$ in cell $C_{ij}$. Alternatively, we may use the Lax–Friedrichs flux:

$$\begin{aligned} \hat{f}\left(u\left(x^\beta_{i+\frac{1}{2}}, \tilde{y}^\alpha_j\right)^-, u\left(x^\beta_{i+\frac{1}{2}}, \tilde{y}^\alpha_j\right)^+\right) = \frac{1}{2} a\left(x^\beta_{i+\frac{1}{2}}, \tilde{y}^\alpha_j\right) \left[u\left(x^\beta_{i+\frac{1}{2}}, \tilde{y}^\alpha_j\right)^- + u\left(x^\beta_{i+\frac{1}{2}}, \tilde{y}^\alpha_j\right)^+\right] \\ + \frac{1}{2}\frac{\delta x}{\delta t}\left[u\left(x^\beta_{i+\frac{1}{2}}, \tilde{y}^\alpha_j\right)^- - u\left(x^\beta_{i+\frac{1}{2}}, \tilde{y}^\alpha_j\right)^+\right]. \end{aligned} \tag{22}$$

We denote by $\hat{g}$, the equivalent fluxes when $a$ is replaced by $b$ and the roles of $x$ and $y$ are interchanged. In this way we obtain the scheme

$$\begin{aligned} \frac{\mathrm{d}\,\overline{\overline{u}}_{ij}}{\mathrm{d}t} = &-\frac{1}{\delta x}\left[\hat{f}_{i+\frac{1}{2},j} - \hat{f}_{i-\frac{1}{2},j}\right] - \frac{1}{\delta y}\left[\hat{g}_{i,j+\frac{1}{2}} - \hat{g}_{i,j-\frac{1}{2}}\right] \\ &+ \frac{d}{\delta x^2}\sum_{\alpha=1}^{5} \tilde{w}_\alpha \left[u(x_{i+1}, \tilde{y}^\alpha_j) - 2u(x_i, \tilde{y}^\alpha_j) + u(x_{i-1}, \tilde{y}^\alpha_j)\right] \\ &+ \frac{d}{\delta y^2}\sum_{\alpha=1}^{5} \tilde{w}_\alpha \left[u(\tilde{x}^\alpha_i, y_{j+1}) - 2u(\tilde{x}^\alpha_i, y_j) + u(\tilde{x}^\alpha_i, y_{j-1})\right] \\ &+ \sum_{\alpha=1}^{5}\sum_{\beta=1}^{5} \tilde{w}_\alpha \tilde{w}_\beta h(\tilde{x}^\alpha_i, \tilde{y}^\beta_j), \end{aligned} \tag{23}$$

where $\hat{f}_{i+\frac{1}{2},j} = \sum_{\alpha=1}^{5}\sum_{\beta=1}^{3} \tilde{w}_\alpha w_\beta \hat{f}(u(x^\beta_{i+\frac{1}{2}}, \tilde{y}^\alpha_j)^-, u(x^\beta_{i+\frac{1}{2}}, \tilde{y}^\alpha_j)^+)$ and $\hat{g}_{i,j+\frac{1}{2}} = \sum_{\alpha=1}^{5}\sum_{\beta=1}^{3} \tilde{w}_\alpha w_\beta \hat{g}(u(\tilde{x}^\alpha_i, y^\beta_{j+\frac{1}{2}})^-, u(\tilde{x}^\alpha_i, y^\beta_{j-\frac{1}{2}})^+)$.

**Step 4. Integrate in time**. The time discretization strategy for (23) defines the order of the scheme in time. Forward Euler schemes are the simple choice leading to order one, which provides stability and positivity. Knowing the right hand $r_{ij}$ side of (23) at time $t_n$, the double average $\overline{\overline{u}}_{ij}(t_{n+1}) = \overline{\overline{u}}_{ij}(t_n) + \delta t\, r_{ij}(t_n)$. The next steps allow approximating the values of $u$ at the nodes at time $t_{n+1}$ and the process is repeated at subsequent times. Higher order time discretizations must belong to the SSP class as discussed in the next section.

**Step 5**. The reconstruction of the required approximations of $u$ from the double averages $\overline{\overline{u}}_{ij}$, is done dimension by dimension, following a procedure detailed in [43]. We recall the procedure in an Appendix for the ease of the reader. Additionally, slope limiters can be enforced as described in [43], if necessary. The scheme is expected to be stable when

$$\left(\frac{\delta t}{\delta x} + \frac{\delta t}{\delta y}\right) \max|a|, |b| \leq \frac{1}{2}\hat{w}_1 \min\{w_1, w_2, w_3\} = \frac{1}{2}\frac{1}{12}\frac{5}{18} = 1 \times 10^{-2}, \tag{24}$$

$$\left(\frac{\delta t}{\delta x^2}+\frac{\delta t}{\delta y^2}\right)\max|\mathrm{d}|\le\frac{1}{4}\tilde{w}_3=\frac{1}{4}\frac{114}{324}=8\times10^{-2}. \tag{25}$$

# 4 Strong stability preserving time discretization

To maintain positivity and stability, we work with SSP time discretizations. High order time discretizations of Runge–Kutta type increase the cost since several evaluations of the right hand side are required per time step. Multistep schemes avoid this problem of reusing the previous step, but increase storage needs and usually require smaller time steps to ensure stability. In spite of their theoretical order, WENO5 schemes might degenerate to order two in practice, in smooth regions. Therefore, we will use SSP schemes or order 2 or 3. Usual choices for third order accuracy are a third order SSP multistep method [43]

$$u(t_{n+1})=\frac{16}{27}\left(u(t_n)+3\delta t\, r(u(t_n))\right)+\frac{11}{27}\left(u(t_{n-3})+\frac{12}{11}\delta t\, r(u(t_{n-3}))\right), \tag{26}$$

and a third order Runge–Kutta method [45]

$$\begin{aligned} u^{(1)}&=u(t_n)+\delta t\, r(u(t_n)),\\ u^{(2)}&=\frac{3}{2}u(t_n)+\frac{1}{4}u^{(1)}+\frac{1}{4}\delta t\, r(u^{(1)}),\\ u(t_{n+1})&=\frac{1}{3}u(t_n)+\frac{2}{3}u^{(2)}+\frac{2}{3}\delta t\, r(u^{(2)}). \end{aligned} \tag{27}$$

The stability of SSP discretizations is governed by a CFL number $c$ as follows. If Euler forward time discretization applied to equation $u_t=r(u)$ remains stable under the condition $\delta t\le\delta t_0$, then SSP time discretization is stable when $\delta t\le d\delta t_0$. For the multistep method $d=1/3$ while $d=1$ ($d_{\mathrm{eff}}=1/3$) for the RK3 (27). For second order approximations, the RK2 scheme is

$$\begin{aligned} u^{(1)}&=u(t_n)+\delta t\, r(u(t_n)),\\ u(t_{n+1})&=\frac{1}{2}u(t_n)+\frac{1}{2}u^{(1)}+\frac{1}{2}\delta t\, r(u^{(1)}), \end{aligned} \tag{28}$$

with $d=1$ ($d_{\mathrm{eff}}=1/2$). In our case, the spatial operator $r(u(t_n))$ is the operator obtained discretizing the space variables, time excluded.

The final scheme for our system would read as follows:

- Initialize the scheme applying the RK3 scheme (27) to the spatially discretized versions of Eqs. (8) and (10), according to Section 3, and to Eq. (13). Store the first three steps, for $n=1,2,3$.
- At each $n>3$, apply the multistep scheme (26) to the spatially discretized versions of Eqs. (8) and (10), according to Section 3, and to Eq. (13).

# 5 Numerical tests in two dimensions

In this section, we present numerical solutions of the reduced Eqs. (8)–(13) for appropriate values of the parameters as listed in Table 1. The slab geometry of the advancing angiogenic network is schematized in Figure 1. More precisely, we consider a slab $(0,1)\times\mathbb{R}$ and set $\mathbf{x}=(x_1,x_2)$. To ease the implementation of WENO discretizations, we slightly modify the boundary conditions proposed in the original model [17]. For numerical purposes we truncate the spatial domain and set $\Omega_{\mathbf{x}}=[0,1]\times[-1.5,1.5]$. We impose zero Dirichlet boundary conditions for $C$ at $x_2=\pm1.5$ and $x_1=0$, as well as zero boundary conditions for $\rho$. At $x_1=1$, we use the function

$$g(t,x_2)=c_{\mathrm{L}}(t)\mathrm{e}^{-a^2x_2^2},\quad t>0,\ x_2\in\mathbb{R}, \tag{29}$$

**Table 1:** Dimensionless parameters.

| $\delta_1$ | $\beta$ | $A$ | $\Gamma$ | $\Gamma_1, q_1$ | $\kappa$ | $\chi$ | $\eta$ | $\epsilon$ | $\sigma_v$ |
|---|---|---|---|---|---|---|---|---|---|
| 0.255 | 5.88 | 22.42 | 0.135 | 1 | 0.0045 | 0.002 | 15 | 0.001 | 0.08 |

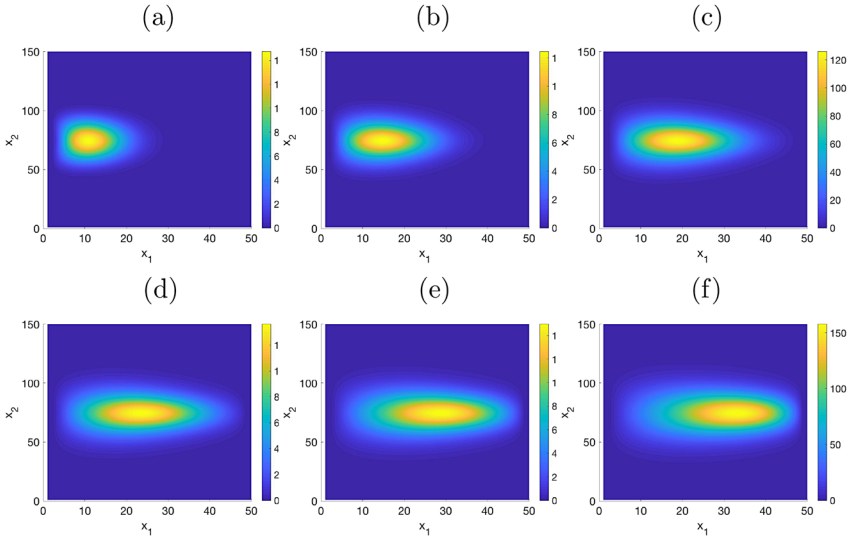


**Figure 2:** Marginal tip density obtained by solving the two dimensional reduced model at times (a) 0.1145, (b) 0.2290, (c) 0.3435, (d) 0.4580, (e) 0.5725 and (f) 0.6870. A soliton-like pattern of new tips forms, which travels from the pre-existing vessel (left) to the hypoxic region releasing the angiogenic factor (right).

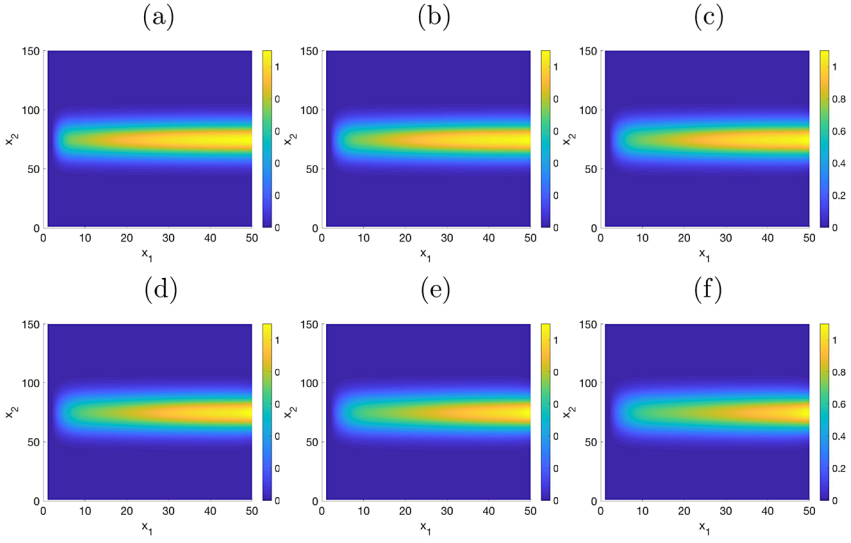


**Figure 3:** Concentration of tumor angiogenic factor obtained solving the two dimensional reduced model at times (a) 0.1145, (b) 0.2290, (c) 0.3435, (d) 0.4580, (e) 0.5725 and (f) 0.6870. The spread of the angiogenic factor shrinks as new vessel tips are formed and advance towards the hypoxic region.

to generate boundary values. Here, $c_L(t) > 0$ to represents the influx of the angiogenic factor produced by the core of the hypoxic region and $1/a$ is a characteristic length thereof. This function will decrease with time as new blood vessels reach the tumor. We set in our simulations $a = 1/0.3$ and $c_L(t) = 1.1$.

For the initial data, we consider

$$p(x_1, x_2, v_1, v_2, 0) = \frac{2}{\pi^2}\frac{1}{0.0048}\mathrm{e}^{-\left(\frac{-x_1}{0.06}\right)^2}\sum_{j=1}^{20}\mathrm{e}^{-\left(\frac{x_2-x_2^j}{0.08}\right)^2}\mathrm{e}^{-[(v_1-v_1^0)^2+(v_2-v_2^0)^2]}, \tag{30}$$

$$C(x_1, x_2, 0) = 1.1\mathrm{e}^{-\left[\left(\frac{x_1-1}{1.5}\right)^2+\left(\frac{x_2}{0.3}\right)^2\right]}, \tag{31}$$

where the vessel tip locations $x_2^j = -0.3 + (j-1)\frac{0.6}{19}$, $j = 1, 2, \ldots, 20$, are 20 equispaced values in $[-0.3, 0.3]$, $v_1^0 = cos(\pi/10)$ and $v_2^0 = \sin(\pi/10)$. Initial values for $\rho(\mathbf{x}, 0)$ are obtained by integrating (30) over the truncated computational velocity domain $\Omega_{\mathbf{v}} = [-4, 4]^2$. The steps are $\delta x = 0.02$ and $\delta t = 2.2906 \times 10^{-4}$.

Figures 2 and 3 show the evolution of the marginal tip density $\rho$ and the angiogenic factor concentration. Note that we only plot the density of tips, not the full vessels already formed that lie behind them, between the pre-existing vessel and the new tips.

# 6 Conclusions

We have introduced a high order positivity preserving scheme for asymptotic reductions of kinetic models of angiogenesis, combining positivity preserving high order WENO discretizations in space and SSP discretization in time. The resulting schemes reproduce traveling patterns representing the formation and spread of blood vessel tips in the direction of a hypoxic region in need of oxygen supply. This approach provides building blocks to devise high order positivity preserving schemes for the full kinetic models by resorting to fractional step splitting schemes [47, 48]. The proper implementation of such schemes is, at present, a computational challenge, out of the scope of the present study.

**Author contribution:** All the authors have accepted responsibility for the entire content of this submitted manuscript and approved submission.
**Research funding:** This research has been partially supported by the FEDER/Ministerio de Ciencia, Innovación y Universidades-Agencia Estatal de Investigación grant no. MTM2017-84446-C2-1-R.
**Conflict of interest statement:** The authors declare no conflicts of interest regarding this article.

# Appendix

## Reconstruction from averages

For the ease of the reader, we sketch here the WENO5 reconstruction procedure of the required approximations of $u$ from the double averages $\overline{\overline{u}}_{ij}$, taken from the detailed description in [43]. This is done dimension by dimension. Let us first recall how to reconstruct a function $u$ of one variable $x$ from the double averages $\overline{\overline{u}}_{i-2}$, $\overline{\overline{u}}_{i-1}$, $\overline{\overline{u}}_i$, $\overline{\overline{u}}_{i+1}$, $\overline{\overline{u}}_{i+2}$, in the variable $x$ at stencils $\mathcal{S}$ formed by intervals $I_{i-2}, I_{i-1}, I_i, I_{i+1}, I_{i+2}$ with $I_i = [x_{i-\frac{1}{2}}, x_{i+\frac{1}{2}}]$. The coefficients of a polynomial $p(x) = \sum_{\ell=0}^{4} c_\ell \left(\frac{x-x_i}{\delta x}\right)^\ell$ satisfying

$$\overline{\overline{u}}_j = \frac{1}{\delta x^2}\int_{x_{j-\frac{1}{2}}}^{x_{j+\frac{1}{2}}}\int_{x-\frac{\delta x}{2}}^{x+\frac{\delta x}{2}} p(\xi)\mathrm{d}\xi\,\mathrm{d}x, \quad j = i-2, \ldots, i+2, \tag{32}$$

are given by

$$\begin{aligned}
c_0 &= \frac{1}{180}(2\bar{\bar{u}}_{i-2} - 23\bar{\bar{u}}_{i-1} + 222\bar{\bar{u}}_i - 23\bar{\bar{u}}_{i+1} + 2\bar{\bar{u}}_{i+2}),\\
c_1 &= \frac{1}{8}(\bar{\bar{u}}_{i-2} - 6\bar{\bar{u}}_{i-1} + 6\bar{\bar{u}}_{i+1} - \bar{\bar{u}}_{i+2}),\\
c_2 &= \frac{1}{12}(-\bar{\bar{u}}_{i-2} + 10\bar{\bar{u}}_{i-1} - 18\bar{\bar{u}}_i + 10\bar{\bar{u}}_{i+1} - \bar{\bar{u}}_{i+2}),\\
c_3 &= \frac{1}{12}(-\bar{\bar{u}}_{i-2} + 2\bar{\bar{u}}_{i-1} - 2\bar{\bar{u}}_{i+1} + \bar{\bar{u}}_{i+2}),\\
c_4 &= \frac{1}{24}(\bar{\bar{u}}_{i-2} - 4\bar{\bar{u}}_{i-1} + 6\bar{\bar{u}}_i - 4\bar{\bar{u}}_{i+1} + \bar{\bar{u}}_{i+2}).
\end{aligned} \tag{33}$$

In terms of linear weights $d_m(x)$, $m = 0, 1, 2$, this polynomial is decomposed as

$$\begin{aligned}
p(x) &= \sum_{m=0}^{2} d_m(x) p_m(x),\\
p_0(x) &= \frac{1}{12}(-\bar{\bar{u}}_{i-2} + 2\bar{\bar{u}}_{i-1} + 11\bar{\bar{u}}_i) + \frac{1}{2}(\bar{\bar{u}}_{i-2} - 4\bar{\bar{u}}_{i-1} + 3\bar{\bar{u}}_i)\left(\frac{x - x_i}{\delta x}\right)\\
&\quad + \frac{1}{2}(\bar{\bar{u}}_{i-2} - 2\bar{\bar{u}}_{i-1} + \bar{\bar{u}}_i)\left(\frac{x - x_i}{\delta x}\right)^2,\\
p_1(x) &= \frac{1}{12}(-\bar{\bar{u}}_{i-1} + 14\bar{\bar{u}}_i - \bar{\bar{u}}_{i+1}) + \frac{1}{2}(-\bar{\bar{u}}_{i-1} + \bar{\bar{u}}_{i+1})\left(\frac{x - x_i}{\delta x}\right)\\
&\quad + \frac{1}{2}(\bar{\bar{u}}_{i-1} - 2\bar{\bar{u}}_i + \bar{\bar{u}}_{i+1})\left(\frac{x - x_i}{\delta x}\right)^2,\\
p_2(x) &= \frac{1}{12}(11\bar{\bar{u}}_i + 2\bar{\bar{u}}_{i+1} - \bar{\bar{u}}_{i+2}) + \frac{1}{2}(-3\bar{\bar{u}}_i + 4\bar{\bar{u}}_{i+1} - \bar{\bar{u}}_{i+2})\left(\frac{x - x_i}{\delta x}\right)\\
&\quad + \frac{1}{2}(\bar{\bar{u}}_i - 2\bar{\bar{u}}_{i+1} + \bar{\bar{u}}_{i+2})\left(\frac{x - x_i}{\delta x}\right)^2.
\end{aligned} \tag{34}$$

Imposing $\sum_{m=0}^{2} d_m(x) = 1$, these weights are listed in Tables 2.1 and 2.2 of reference [43] for the points $x^{\alpha}_{i\pm\frac{1}{2}}$, $\alpha = 1, 2, 3$ and $\tilde{x}^{\alpha}_i$, $\alpha = 1, \dots, 5$ we use (see Table 2 here). Some of these linear weights are negative and may lead to instability. In practice, they are replaced by normalized nonlinear weights $\omega_m$. When at a point $x$ the three linear weights $d_m(x)$ are positive, we set

$$\begin{aligned}
\omega_m(x) &= \frac{\tilde{\omega}_m(x)}{\sum_{\ell=0}^{2} \tilde{\omega}_\ell(x)}, \quad \tilde{\omega}_m(x) = \frac{d_m(x)}{(\beta_m + \varepsilon)^2},\\
\beta_0 &= \frac{13}{12}(\bar{\bar{u}}_{i-2} - 2\bar{\bar{u}}_{i-1} + \bar{\bar{u}}_i)^2 + \frac{1}{4}(\bar{\bar{u}}_{i-2} - 4\bar{\bar{u}}_{i-1} + 3\bar{\bar{u}}_i)^2,\\
\beta_1 &= \frac{13}{12}(\bar{\bar{u}}_{i-1} - 2\bar{\bar{u}}_i + \bar{\bar{u}}_{i+1})^2 + \frac{1}{4}(\bar{\bar{u}}_{i-1} - 3\bar{\bar{u}}_{i+1})^2,\\
\beta_2 &= \frac{13}{12}(\bar{\bar{u}}_i - 2\bar{\bar{u}}_{i+1} + \bar{\bar{u}}_{i+2})^2 + \frac{1}{4}(3\bar{\bar{u}}_i - 4\bar{\bar{u}}_{i+1} + 3\bar{\bar{u}}_{i+2})^2,
\end{aligned} \tag{35}$$

for $\varepsilon > 0$ small (typically $\varepsilon = 10^{-6}$) and $m = 0, 1, 2$. If any of the weights is negative at $x$, we define $\omega_m(x)$ as follows:

$$\begin{aligned}
\omega_m(x) &= \sigma^+(x)\omega_m^+(x) - \sigma^-(x)\omega_m^-(x), \quad \sigma^{\pm}(x) = \sum_{\ell=0}^{2} \tilde{\gamma}_\ell^{\pm}(x),\\
\omega_m^{\pm}(x) &= \frac{\tilde{\omega}_m^{\pm}(x)}{\sum_{\ell=0}^{2} \tilde{\omega}_\ell^{\pm}(x)}, \quad \tilde{\omega}_m^{\pm}(x) = \frac{\gamma_m^{\pm}(x)}{(\beta_m + \varepsilon)^2},\\
\gamma_m^{\pm}(x) &= \frac{\tilde{\gamma}_m^{\pm}(x)}{\sigma^{\pm}(x)},\ \tilde{\gamma}_m^{+}(x) = \frac{1}{2}(d_m(x) + \theta|d_m(x)|),\ \tilde{\gamma}_m^{-}(x) = \tilde{\gamma}_m^{+}(x) - d_m(x),
\end{aligned} \tag{36}$$

**Table 2:** Linear weights $d_m(x)$ for typical point choices.

| $x$ | $d_1(x)$ | $d_2(x)$ | $d_3(x)$ |
|---|---|---|---|
| $x_{i-\frac{1}{2}} - \frac{\sqrt{15}}{10}\delta x$ | $\frac{307+72\sqrt{15}}{960}$ | $\frac{8377-1542\sqrt{15}}{6720}$ | $\frac{173(-11+3\sqrt{15})}{3360}$ |
| $x_{i-\frac{1}{2}}$ | $\frac{341}{1200}$ | $\frac{337}{600}$ | $\frac{37}{240}$ |
| $x_{i-\frac{1}{2}} + \frac{\sqrt{15}}{10}\delta x$ | $\frac{307-72\sqrt{15}}{960}$ | $\frac{8377+1542\sqrt{15}}{6720}$ | $-\frac{173(11+3\sqrt{15})}{3360}$ |
| $x_{i+\frac{1}{2}} - \frac{\sqrt{15}}{10}\delta x$ | $-\frac{173(11+3\sqrt{15})}{3360}$ | $\frac{8377+1542\sqrt{15}}{6720}$ | $\frac{307-72\sqrt{15}}{960}$ |
| $x_{i+\frac{1}{2}}$ | $\frac{37}{240}$ | $\frac{337}{600}$ | $\frac{341}{1200}$ |
| $x_{i+\frac{1}{2}} + \frac{\sqrt{15}}{10}\delta x$ | $\frac{173(-11+3\sqrt{15})}{3360}$ | $\frac{8377-1542\sqrt{15}}{6720}$ | $\frac{307+72\sqrt{15}}{960}$ |
| $x_i - \frac{\sqrt{10}}{5}\delta x$ | $\frac{427+87\sqrt{15}}{1590}$ | $\frac{368}{795}$ | $\frac{427-87\sqrt{15}}{590}$ |
| $x_i - \frac{\sqrt{10}}{10}\delta x$ | $\frac{29147-246\sqrt{15}}{129360}$ | $\frac{35533}{64680}$ | $\frac{29147+246\sqrt{15}}{129360}$ |
| $x_i$ | $-\frac{2}{15}$ | $\frac{19}{15}$ | $-\frac{2}{15}$ |
| $x_i + \frac{\sqrt{10}}{10}\delta x$ | $\frac{29147+246\sqrt{15}}{129360}$ | $\frac{35533}{64680}$ | $\frac{29147-246\sqrt{15}}{129360}$ |
| $x_i + \frac{\sqrt{10}}{5}\delta x$ | $\frac{427-87\sqrt{15}}{1590}$ | $\frac{368}{795}$ | $\frac{427+87\sqrt{15}}{1590}$ |

for $\theta = 3$ and $m = 0, 1, 2$. Once this is done, the polynomial approximation of $u$ in $S$ obtained from the double averages is

$$p(x) = \sum_{m=0}^{2} \omega_m(x) d_m(x). \tag{37}$$

The procedure to reconstruct a two dimensional function at the required points is as follows:

- For $u(x^{\beta}_{i+\frac{1}{2}}, \tilde{y}^{\alpha}_j)^-$ and $u(x^{\beta}_{i-\frac{1}{2}}, \tilde{y}^{\alpha}_j)^+$
  - Fix $\tilde{y}^{\alpha}_j$, $\alpha = 1, \dots, 5$ and apply (32)–(37) to reconstruct the one-dimensional double averages $\overline{\overline{u}}_i(\tilde{y}^{\alpha}_j)$ in the $x$ direction from the values $\overline{\overline{u}}_{i,j-2}$, $\overline{\overline{u}}_{i,j-1}$, $\overline{\overline{u}}_{i,j}$, $\overline{\overline{u}}_{i,j+1}$, $\overline{\overline{u}}_{i,j+2}$.
  - Next, apply (32)–(37) to reconstruct $u$ at the points $(x^{\beta}_{i\pm\frac{1}{2}}, \tilde{y}^{\alpha}_j)$ for $\beta = 1, 2, 3$ from the values values $\overline{\overline{u}}_{i-2}(\tilde{y}^{\alpha}_j)$, $\overline{\overline{u}}_{i-1}(\tilde{y}^{\alpha}_j)$, $\overline{\overline{u}}_{i}(\tilde{y}^{\alpha}_j)$, $\overline{\overline{u}}_{i+1}(\tilde{y}^{\alpha}_j)$, $\overline{\overline{u}}_{i+2}(\tilde{y}^{\alpha}_j)$.
- For $u(\tilde{x}^{\alpha}_i, y^{\beta}_{j+\frac{1}{2}})^-$ and $u(\tilde{x}^{\alpha}_i, y^{\beta}_{j-\frac{1}{2}})^+$
  - Fix $\tilde{x}^{\alpha}_i$, $\alpha = 1, \dots, 5$ and apply (32)–(37) to reconstruct the one dimensional double averages $\overline{\overline{u}}_j(\tilde{x}^{\alpha}_i)$ in the $y$ direction from the values $\overline{\overline{u}}_{i-2,j}$, $\overline{\overline{u}}_{i-1,j}$, $\overline{\overline{u}}_{i,j}$, $\overline{\overline{u}}_{i+1,j}$, $\overline{\overline{u}}_{i+2,j}$.
  - Next, apply (32)–(37) to reconstruct $u$ at the points $(\tilde{x}^{\alpha}_i, y^{\beta}_{j\pm\frac{1}{2}})$ for $\beta = 1, 2, 3$ from the values $\overline{\overline{u}}_{j-2}(\tilde{x}^{\alpha}_i)$, $\overline{\overline{u}}_{j-1}(\tilde{x}^{\alpha}_i)$, $\overline{\overline{u}}_{j}(\tilde{x}^{\alpha}_i)$, $\overline{\overline{u}}_{j+1}(\tilde{x}^{\alpha}_i)$, $\overline{\overline{u}}_{j+2}(\tilde{x}^{\alpha}_i)$.
- For $u(x_i, \tilde{y}^{\alpha}_j)$
  - Fix $x_i$ and apply (32)–(37) to reconstruct the one dimensional double averages $\overline{\overline{u}}_j(x_i)$ in the $y$ direction from the values $\overline{\overline{u}}_{i-2,j}$, $\overline{\overline{u}}_{i-1,j}$, $\overline{\overline{u}}_{i,j}$, $\overline{\overline{u}}_{i+1,j}$, $\overline{\overline{u}}_{i+2,j}$.
  - Next, apply (32)–(37) to reconstruct $u$ at the points $(x_i, \tilde{y}^{\alpha}_j)$ for $\alpha = 1, \dots, 5$ from the values $\overline{\overline{u}}_{j-2}(x_i)$, $\overline{\overline{u}}_{j-1}(x_i)$, $\overline{\overline{u}}_{j}(x_i)$, $\overline{\overline{u}}_{j+1}(x_i)$, $\overline{\overline{u}}_{j+2}(x_i)$.
- For $u(\tilde{x}^{\alpha}_i, y_j)$
  - Fix $y_j$ and apply (32)–(37) to reconstruct the one dimensional double averages $\overline{\overline{u}}_i(y_j)$ in the $x$ direction from the values $\overline{\overline{u}}_{i,j-2}$, $\overline{\overline{u}}_{i,j-1}$, $\overline{\overline{u}}_{i,j}$, $\overline{\overline{u}}_{i,j+1}$, $\overline{\overline{u}}_{i,j+2}$.
  - Next, apply (32)–(37) to reconstruct $u$ at the points $u(\tilde{x}^{\alpha}_i, y_j)$ for $\alpha = 1, \dots, 5$ from the values $\overline{\overline{u}}_{i-2}(y_j)$, $\overline{\overline{u}}_{i-1}(y_j)$, $\overline{\overline{u}}_{i}(y_j)$, $\overline{\overline{u}}_{i+1}(y_j)$, $\overline{\overline{u}}_{i+2}(y_j)$.

# References


[1] P. F. Carmeliet, "Angiogenesis in life, disease and medicine," *Nature*, vol. 438, pp. 932–936, 2005.

[2] J. Folkman, "Tumor angiogenesis. Therapeutic implications," *N. Engl. J. Med.*, vol. 285, pp. 1182–1186, 1971.

[3] K. R. Swanson, R. C. Rockne, J. Claridge, M. A. Chaplain, E. C. Alvord Jr, and A. R. A. Anderson, "Quantifying the role of angiogenesis in malignant progression of gliomas: in silico modeling integrates imaging and histology," *Cancer Res.*, vol. 71, pp. 7366–7375, 2011.

[4] P. F. Carmeliet and R. K. Jain, "Molecular mechanisms and clinical applications of angiogenesis," *Nature*, vol. 473, pp. 298–307, 2011.

[5] M. Scianna, L. Munaron, and L. Preziosi, "A multiscale hybrid approach for vasculogenesis and related potential blocking therapies," *Prog. Biophys. Mol. Biol.*, vol. 106, pp. 450–462, 2011.

[6] L. Yadav, N. Puri, V. Rastogi, P. Satpute, and V. Sharma, "Tumour angiogenesis and angiogenic inhibitors: a review," *J. Clin. Diagn. Res.*, vol. 9, pp. XE01–XE05, 2015.

[7] B. M. Prior, H. T. Yang, and R. L. Terjung, "What makes vessels grow with exercise training?" *J. Appl. Physiol.*, vol. 97, no. 3, pp. 1119–28, 2004.

[8] T. A. M. Heck, M. M. Vaeyens, and H. Van Oosterwyck, "Computational models of sprouting angiogenesis and cell migration: towards multiscale mechanochemical models of angiogenesis," *Math. Model Nat. Phenom.*, vol. 10, p. 09735348, 2015.

[9] F. Milde, M. Bergdorf, and P. Koumoutsakos, "A hybrid model for three-dimensional simulations of sprouting angiogenesis," *Biophys. J.*, vol. 95, pp. 3146–3160, 2008.

[10] S. M. Peirce, "Computational and mathematical modeling of angiogenesis," *Microcirculation*, vol. 15, no. 8, pp. 739–751, 2008.

[11] M. Scianna, C. G. Bell, and L. Preziosi, "A review of mathematical models for the formation of vascular networks," *J. Theor. Biol.*, vol. 333, pp. 174–209, 2013.

[12] S. Sun, M. F. Wheeler, M. Obeyesekere, and Ch. Patrick Jr, "Multiscale angiogenesis modeling using mixed finite element methods," *Multiscale Model. Simul.*, vol. 4, no. 4, pp. 1137–1167, 2005.

[13] F. Terragni, M. Carretero, V. Capasso, and L. L. Bonilla, "Stochastic model of tumor-induced angiogenesis: ensemble averages and deterministic equations," *Phys. Rev.*, vol. 93, p. 022413, 2016.

[14] A. Carpio, G. Duro, and M. Negreanu, "Constructing solutions for a kinetic model of angiogenesis in annular domains," *Appl. Math. Model.*, vol. 45, pp. 303–322, 2017.

[15] A. Carpio and G. Duro, "Well posedness of an integrodifferential kinetic model of Fokker-Planck type for angiogenesis," *Nonlinear Anal. R. World Appl.*, vol. 30, pp. 184–212, 2016.

[16] L. L. Bonilla, M. Carretero, and F. Terragni, "Solitonlike attractor for blood vessel tip density in angiogenesis," *Phys. Rev.*, vol. 94, p. 062415, 2016.

[17] L. L. Bonilla, A. Carpio, M. Carretero, G. Duro, and F. M. Negreanu, "Terragni A convergent numerical scheme for integrodifferential kinetic models of angiogenesis," *J. Comput. Phys.*, vol. 375, pp. 1270–1294, 2018.

[18] V. Capasso, D. Morale, and G. Facchetti, "Randomness in self-organized phenomena. A case study: retinal angiogenesis," *Biosystems*, vol. 112, pp. 292–297, 2013.

[19] M. Asadzadeh and P. Kowalczyk, "Convergence analysis of the streamline diffusion and discontinuous Galerkin methods for the Vlasov-Fokker-Planck system," *Numer. Methods Part. Differ. Equ.*, vol. 21, pp. 472–495, 2005.

[20] M. Asadzadeh and A. Sopasakis, "Convergence of a hp-streamline diffusion scheme for Vlasov-Fokker-Planck system," *Math. Model Methods Appl. Sci.*, vol. 17, no. 8, pp. 1159–1182, 2007.

[21] R. J. Kingham and A. R. Bell, "An implicit Vlasov-Fokker-Planck code to model non-local electron transport in 2-D with magnetic fields," *J. Comput. Phys.*, vol. 194, no. 1, pp. 1–34, 2004.

[22] K. J. Havlak and H. D. Victory Jr, "The numerical analysis of random particle methods applied to Vlasov-Poisson-Fokker-Planck kinetic equations," *SIAM J. Numer. Anal.*, vol. 33, pp. 291–317, 1996.

[23] K. J. Havlak and H. D. Victory Jr, "On deterministic particle methods for solving Vlasov-Poisson-Fokker-Planck systems," *SIAM J. Numer. Anal.*, vol. 35, no. 4, pp. 1473–1519, 1998.

[24] S. Wollman and E. Ozizmir, "Numerical approximation of the Vlasov-Poisson-Fokker-Planck system in two dimensions," *J. Comput. Phys.*, vol. 228, pp. 6629–6669, 2009.

[25] P. Degond, L. Pareschi, and G. Russo, *Modeling and Computational Methods for Kinetic Equations*, Birkhauser Basel Boston, 2004.

[26] L. Einkemmer, "Splitting methods for Vlasov-Poisson and Vlasov-Maxwell equations," PhD thesis, University of Innsbruck, 2014.

[27] J. M. Qiu and A. Christlieb, "A conservative high order semi-Lagrangian WENO method for the Vlasov equation," *J. Comput. Phys.*, vol. 229, no. 4, pp. 1130–1149, 2010.

[28] D. Seal, "Discontinuous Galerkin methods for Vlasov models of plasma," PhD thesis, University of Wisconsin-Madison, 2012.

[29] F. Filbet, E. Sonnendrücker, and P. Bertrand, "Conservative numerical schemes for the Vlasov equation," *J. Comput. Phys.*, vol. 172, pp. 166–187, 2001.
[30] F. Filbet and E. Sonnendrücker, "Comparison of Eulerian Vlasov solvers," *Comput. Phys. Commun.*, vol. 150, no. 3, pp. 247–266, 2003.
[31] G. H. Cottet and P. A. Raviart, "Particle methods for the one-dimensional Vlasov-Poisson equations," *SIAM J. Numer. Anal.*, vol. 21, pp. 52–76, 1984.
[32] B. Wang, G. H. Miller, and P. Colella, "A particle-in-cell method with adaptive phase-space remapping for kinetic plasmas," *SIAM J. Sci. Comput.*, vol. 33, no. 6, pp. 3509–3537, 2011.
[33] E. Sonnendrücker, J. Roche, P. Bertrand, and A. Ghizzo, "The semi-Lagrangian method for the numerical resolution of Vlasov equations," *J. Comput. Phys.*, vol. 149, no. 2, pp. 201–220, 1999.
[34] C. Z. Cheng and G. Knorr, "The integration of the Vlasov equation in configuration space," *J. Comput. Phys.*, vol. 22, pp. 330–351, 1976.
[35] B. Sepehrian and M. K. Radpoor, "Numerical solution of non-linear Fokker-Planck equation using finite differences method and the cubic spline functions," *Appl. Math. Comput.*, vol. 262, pp. 187–190, 2015.
[36] L. Chacón, D. C. Barnes, D. A. Knoll, and G. H. Miley, "An implicit energy-conservative 2D Fokker-Planck algorithm: I. difference scheme," *J. Comput. Phys.*, vol. 157, no. 2, pp. 618–653, 2000.
[37] A. Marquina, "Diffusion front capturing schemes for a class of Fokker-Planck equations: application to the relativistic heat equation," *J. Comput. Phys.*, vol. 229, no. 7, pp. 2659–2674, 2010.
[38] C. Buet, S. Cordier, P. Degond, and M. Lemou, "Fast algorithms for numerical, conservative, and entropy approximations of the Fokker-Planck-Landau equation," *J. Comput. Phys.*, vol. 133, no. 2, pp. 310–322, 1997.
[39] W. T. Taitano, L. Chacón, A. N. Simakov, and K. Molvig, "A mass, momentum, and energy conserving, fully implicit, scalable algorithm for the multi-dimensional, multi-species Rosenbluth-Fokker-Planck equation," *J. Comput. Phys.*, vol. 297, no. 1, pp. 357–380, 2015.
[40] J. W. Banks and J. A. F. Hittinger, "A new class of nonlinear finite-volume methods for Vlasov simulation," *IEEE Trans. Plasma Sci.*, vol. 38, no. 9, pp. 2198–2207, 2010.
[41] S. Tanaka, K. Yoshikawa, T. Minoshima, and N. Yoshida, "Multidimensional Vlasov-Poisson simulations with high-order monotonicity and positivity-preserving schemes," *Astrophys. J.*, vol. 849, p. 76, 2017.
[42] M. Dehghan and M. Abbaszadeh, "A local meshless method for solving multi-dimensional Vlasov-Poisson and Vlasov-Poisson-Fokker-Planck systems arising in plasma physics," *Eng. Comput.*, vol. 33, pp. 961–981, 2017.
[43] X. Zhang, Y. Liu, and C. W. Shu, "Maximum-principle-satisfying high order finite volume weighted essentially nonoscillatory schemes for convection-diffusion equations," *SIAM J. Sci. Comput.*, vol. 34, no. 2, pp. A627–A658, 2012.
[44] C. W. Shu and S. Osher, "Efficient implementation of essentially non-oscillatory shock capturing schemes," *J. Comput. Phys.*, vol. 77, pp. 439–471, 1988.
[45] C. W. Shu, "Total-variation diminishing time discretizations," *SIAM J. Sci. Stat. Comput.*, vol. 9, pp. 1073–1084, 1988.
[46] S. J. Ruuth and W. Hundsdorfer, "High-order linear multistep methods with general monotonicity and boundedness properties," *J. Comput. Phys.*, vol. 209, pp. 226–248, 2005.
[47] H. Jia and K. Li, "A third accurate operator splitting method," *Math. Comput. Model.*, vol. 53, pp. 387–396, 2011.
[48] I. Farago, A. Havasi, and R. Horvath, "On the order of operator splitting methods for time-dependent linear systems of differential equations," *International Journal of Numerical Analysis and Modeling-Series B*, vol. 2, pp. 142–154, 2011.